



Flux Crystal Growth, Crystal Structure, and Optical Properties of New Germanate Garnet $\text{Ce}_2\text{CaMg}_2\text{Ge}_3\text{O}_{12}$

Jie Chen^{1,2}, Hong Yan^{1,2}, Akihide Kuwabara³, Mark D. Smith⁴, Yuki Iwasa⁵, Hiraku Ogino⁵, Yoshitaka Matsushita⁶, Yoshihiro Tsujimoto^{1,2,4*}, Kazunari Yamaura^{1,2} and Hans-Conrad zur Loye^{4*}

¹ Research Center for Functional Materials, National Institute for Materials Science, Tsukuba, Japan, ² Graduate School of Chemical Sciences and Engineering, Hokkaido University, Sapporo, Japan, ³ Nanostructures Research Laboratory, Japan Fine Ceramic Center, Nagoya, Japan, ⁴ Department of Chemistry and Biochemistry, University of South Carolina, Columbia, SC, United States, ⁵ Electronics and Photonics Research Institute, National Institute of Advanced Industrial Science and Technology, Tsukuba, Japan, ⁶ Materials Analysis Station, National Institute for Materials Science, Tsukuba, Japan

OPEN ACCESS

Edited by:

Sidney J. L. Ribeiro,
São Paulo State University, Brazil

Reviewed by:

Helene Serier-Brault,
UMR6502 Institut des Matériaux Jean
Rouxel (IMN), France
Eri Sakuda,
Nagasaki University, Japan

*Correspondence:

Yoshihiro Tsujimoto
TSUJIMOTO.Yoshihiro@nims.go.jp
Hans-Conrad zur Loye
zurloye@mailbox.sc.edu

Specialty section:

This article was submitted to
Inorganic Chemistry,
a section of the journal
Frontiers in Chemistry

Received: 28 November 2019

Accepted: 29 January 2020

Published: 18 February 2020

Citation:

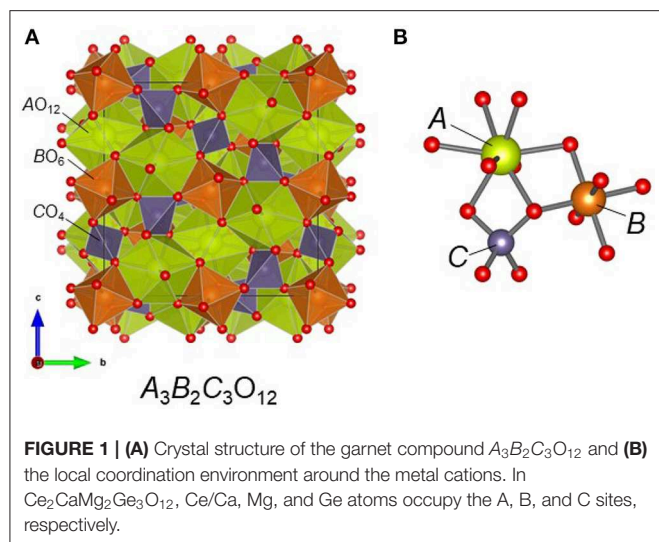
Chen J, Yan H, Kuwabara A,
Smith MD, Iwasa Y, Ogino H,
Matsushita Y, Tsujimoto Y, Yamaura K
and zur Loye H-C (2020) Flux Crystal
Growth, Crystal Structure, and Optical
Properties of New Germanate Garnet
 $\text{Ce}_2\text{CaMg}_2\text{Ge}_3\text{O}_{12}$.
Front. Chem. 8:91.
doi: 10.3389/fchem.2020.00091

A new germanate garnet compound, $\text{Ce}_2\text{CaMg}_2\text{Ge}_3\text{O}_{12}$, was synthesized via flux crystal growth. Truncated spherical, reddish-orange single crystals with a typical size of 0.1–0.3 mm were grown out of a $\text{BaCl}_2\text{-CaCl}_2$ melt. The single crystals were characterized by single-crystal X-ray diffraction analysis, which revealed that it adopted a cubic garnet-type structure with $a = 12.5487(3)$ Å in the space group $la-3d$. Its composition is best described as $\text{A}_3\text{B}_2\text{C}_3\text{O}_{12}$, where Ce/Ca, Mg, and Ge occupied the A, B, and C sites, respectively. A UV-vis absorption spectroscopy measurement on the germanate garnet revealed a clear absorption edge corresponding to a band gap of 2.21 eV ($\lambda = 561$ nm). First-principle calculations indicated that the valence band maximum was composed of Ce 4f bands, whereas the conduction band minimum mainly consisted of Ce 5d bands. These findings explain the observed absorption edge through the Ce 4f \rightarrow 5d absorption. Photoluminescence emission spectra exhibited a very broad peak centered at 600 nm, corresponding to transition from the lowest energy d level to the 4f levels.

Keywords: flux crystal growth, garnet, germanate, single crystal, photoluminescence

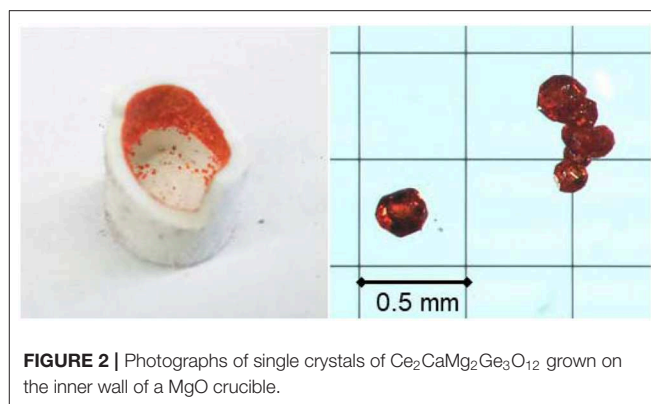
INTRODUCTION

The garnet structure, having the general chemical formula $\{A\}_3\{B\}_2\{C\}_3\text{O}_{12}$, has been widely studied as a host material for various optical applications, such as laser amplifiers, color converters, scintillators, and cathode ray phosphors (Zhiguo and Meijerink, 2017). In particular, the Ce^{3+} -doped $\text{Y}_3\text{Al}_5\text{O}_{12}$ garnet phosphor (YAG:Ce) is one of the most interesting materials in terms of practical application as a blue-to-yellow converter in white-emitting diodes. Although YAG:Ce exhibits good thermal and chemical stability and high luminescence efficiency, improvements to the low thermal quenching temperature and cool correlated color temperature remain significant issues (Bachmann et al., 2009; Shao et al., 2011; Ueda et al., 2015). In principle, the 5d–4f emission bands in Ce^{3+} -doped phosphors are strongly influenced by the host lattice through crystal field splitting of the 5d levels of the Ce^{3+} ion. In the garnet host, there are three types of cation sites: the



{A} site with 8-fold dodecahedral coordination, the [B] site with 6-fold octahedral coordination, and the (C) site with 4-fold tetrahedral coordination (**Figure 1**). The A site is typically occupied by rare-earth (RE) ions such as La^{3+} , Gd^{3+} , or Lu^{3+} , as well as by Y^{3+} , and by alkaline earth ions such as Ca^{2+} . The B site is occupied by smaller ions that prefer octahedral coordination environments, such as Mg^{2+} , Mn^{3+} , Fe^{3+} , Sc^{3+} , Al^{3+} , or Zr^{4+} , while the C site accommodates ions that take on tetrahedral coordination, including Al^{3+} , Ga^{3+} , Si^{4+} , or Ge^{4+} ions. The dodecahedral site, which the trivalent Ce^{3+} ion prefers to occupy, connects to the adjacent A, B, and C sites through common oxygen atoms via corner and edge sharing. Thus, the crystal field impinging on the Ce^{3+} ions is created not only by the A site cations but also the B and C site cations (Setlur et al., 2006; Muñoz-García and Seijo, 2010; Muñoz-García et al., 2010). Owing to the wide range of cations that can be accommodated by the garnet structure, new compositions of garnet phosphors that compensate for the above-mentioned shortcomings of YAG:Ce have been successfully synthesized.

When considering the crystal chemistry of the garnet family, the ability of the cation sites, especially the A site, to accommodate different elements, is an important factor (Geller, 1967). A large number of garnet compounds have been previously reported (Tauber et al., 1958; Reinen, 1964; Lévy and Barbier, 1999; Zhiguo and Meijerink, 2017) but the variety of RE ions in the A site is typically limited to $RE = Gd-Lu$ and Y, all smaller than the desirable Eu^{3+} cation, because incorporation of larger cation causes markedly unfavorable lattice distortions around the dodecahedral sites. To the best of our knowledge, only very few garnet compositions that include early RE ions larger than Gd^{3+} have been synthesized (via various techniques such as the sol-gel method and hydrothermal reaction), and include: $Eu_3Al_5O_{12}$ (Garskaite et al., 2007), $RE_3Te_2Li_3O_{12}$ ($RE = Pr-Eu$) (Kasper, 1969), $RE_3W_2Li_3O_{12}$ ($RE = Pr, Nd$) (Kasper, 1969), $RE_3Fe_5O_{12}$ ($RE = Pr-Eu$) (Dukhovskaya et al., 1973; Komori et al., 2009a,b; Guo et al., 2011), $La_3Sc_2Ga_3O_{12}$



(Malysa et al., 2018), $RE_3Ga_5O_{12}$ ($RE = Pr-Eu$) (Sawada, 1997; Sawada et al., 2016), $Li_7La_3Zr_2O_{12}$ (Awaka et al., 2009), and $Li_5La_3Sb_2O_{12}$ (Murugan et al., 2008). It is notable that even among these, achieving a garnet composition with Ce^{3+} fully occupying the A site is challenging; however, Ce^{3+} doping as high as 56 at.% with respect to Y^{3+} has been achieved in YFe_5O_{12} via the glycothermal process (Rongjin et al., 2013).

In this study, we report the flux crystal growth of the new germanate oxide $\{Ce_2Ca\}[Mg]_2(Ge)_3O_{12}$, which crystallizes in the garnet structure in the space group $1a-3d$ with $a = 12.5487(3)$ Å. The garnet phase was synthesized via the flux crystal growth method where truncated spherical, reddish-orange single crystals were obtained from a $BaCl_2-CaCl_2$ melt. High-temperature solid state reactions failed to yield the target phase, even as a polycrystalline powder, suggesting that the phase is metastable. Herein we discuss the crystal structure, electronic structure, and optical properties of $Ce_2CaMg_2Ge_3O_{12}$.

EXPERIMENTAL

Crystal Growth

Single crystals of $Ce_2CaMg_2Ge_3O_{12}$ were grown via the flux method using a eutectic $BaCl_2-CaCl_2$ mixture (Bugaris and zur Loye, 2012). For $Ce_2CaMg_2Ge_3O_{12}$, a magnesia crucible was loaded with 1 mmol CeO_2 (Aldrich, 4N), 1 mmol of GeO_2 (Rare Metallic, 4N), 1 mmol of S (High Purity Materials, 4N), 3.1 mmol of $BaCl_2$ (Rare Metallic, 3N), and 3.1 mmol of $CaCl_2$ (Rare Metallic, 3N). The top of the crucible was closed with a magnesia cap, and the crucible was sealed inside a silica tube under vacuum. As described later, the magnesia crucible was found to act as a magnesium source. The starting materials were heated in a box furnace to $900^\circ C$ at $150^\circ C/h$, held for 25 h, cooled to $500^\circ C$ at $5^\circ C/h$, and then allowed to cool naturally to room temperature. The products were washed in distilled water, aided by sonication, before the reddish-orange transparent truncated spherical crystals of $Ce_2CaMg_2Ge_3O_{12}$, together with pale-purple transparent crystals of $CeOCl$, were collected via vacuum filtration. The typical dimensions of the single crystals of the garnet compound were $0.3 \times 0.3 \times 0.3 \text{ mm}^3$ (**Figure 2**). The structure of $Ce_2CaMg_2Ge_3O_{12}$ was determined by single-crystal X-ray diffraction analysis.

$\text{Ce}_2\text{CaMg}_2\text{Ge}_3\text{O}_{12}$ single crystals were obtained unintentionally because our original target system was germanium-containing oxysulfide. As described later, sulfur was not incorporated in the garnet structure, and no oxysulfide compounds could be obtained.

Single Crystal Structure Analysis

X-ray intensity data from an orange polyhedron were collected at 301(2) K using a Bruker D8 QUEST diffractometer equipped with a PHOTON 100 CMOS area detector and an Incoatec microfocus source (Mo $K\alpha$ radiation, $\lambda = 0.71073$ Å) (Bruker AXS Inc., 2016). The data collection covered 100% of the reciprocal space to $2\theta_{\text{max}} = 75.2^\circ$, with an average reflection redundancy of 35.3 and $R_{\text{int}} = 0.064$ after absorption correction. The raw area detector data frames were reduced and corrected for absorption effects using the SAINT+ and SADABS programs (Krause et al., 2015; Bruker AXS Inc., 2016). Final unit cell parameters were determined by least-squares refinement of 3812 reflections taken from the data set. An initial structural model was obtained with SHELXT (Sheldrick, 2015). Subsequent difference Fourier calculations and full-matrix least-squares refinement against F^2 were performed with SHELXL-2018 using the ShelXle interface (Hübschle et al., 2011).

Solid State Synthesis

The synthesis of polycrystalline powder samples of $\text{Ce}_2\text{CaMg}_2\text{Ge}_3\text{O}_{12}$ was attempted using CeO_2 , CaCO_3 (or CaO), MgO , and GeO_2 in a stoichiometric ratio. The mixture was ground intimately, pelletized, and heated in a flowing N_2 or H_2 (20%)– Ar (80%) mixed gas atmosphere or in an evacuated sealed tube using a tubular furnace at temperatures ranging from 900 to 1,300°C.

XRD, UV-vis, PL, PLE, and Magnetic Measurements

Single crystals of $\text{Ce}_2\text{CaMg}_2\text{Ge}_3\text{O}_{12}$ were crushed with an agate mortar and pestle to obtain fine powders used for obtaining synchrotron X-ray powder diffraction (SXRD) patterns, UV-vis diffuse reflectance spectra, and photoluminescence (PL) and photoluminescence excitation (PLE) spectra. The products obtained via solid state reactions were examined at room temperature by powder XRD analysis using a Rigaku MiniFlex X-ray diffractometer (Cu $K\alpha$ radiation) in the 2θ range of 5 – 65° with a step size of 0.04° . SXRD measurement was performed at room temperature using a one-dimensional detector installed on BL15XU, NIMS beamline at SPring-8 in Japan. The synchrotron radiation X-rays were monochromatized to a wavelength of 0.65298 Å. The $\text{Ce}_2\text{CaMg}_2\text{Ge}_3\text{O}_{12}$ powder sample was loaded into a 0.1-mm diameter glass capillary. The diffraction data were recorded in 0.003° increments over the range 2 – 60° and analyzed by Rietveld refinement using the program RIETAN-FP (Izumi and Momma, 2007). Diffuse reflectivity measurements were performed at room temperature using a Shimadzu UV-2600 spectrophotometer equipped with an ISR-2600Plus integration sphere. The diffuse reflectance data were internally converted to absorbance by the instrument using the Kubelka–Munk function. The PLE and emission spectra

were recorded using a fluorescence spectrophotometer (Hitachi F-7000). The magnetic susceptibility of $\text{Ce}_2\text{CaMg}_2\text{Ge}_3\text{O}_{12}$ was measured using a SQUID magnetometer (Quantum Design, MPMS-XL). The crushed single crystals were measured at an applied magnetic field (H) of 1 kOe in the range of 10–300 K under both zero-field-cooled (ZFC) and field-cooled (FC) conditions.

First-Principles Calculations

First-principles total energy calculations of $\text{Ce}_2\text{CaMg}_2\text{Ge}_3\text{O}_{12}$ were performed using the projector augmented wave method (Blöchl, 1994; Kresse and Joubert, 1999) as implemented in the Vienna Ab-initio Simulation Package (VASP) (Kresse and Hafner, 1993; Kresse and Furthmüller, 1996a,b). In the present study, the cut-off energy for the plane wave basis was 550 eV. The exchange-correlation interaction potentials of electrons were handled within a framework of the generalized gradient approximation (GGA) of with the PBEsol type (Perdew et al., 2008). The configurations of the valence electrons of Ce, Ca, Mg, Ge and O were $5s^2 5p^6 4f^1 5d^1 6s^2$, $3s^2 3p^6 4s^2$, $2p^6 3s^2$, $3d^{10} 4s^2 4p^2$, and $2s^2 2p^4$, respectively. Spin-polarized calculations were carried out. For Ce ions, the effect of the strong correlation interaction of the 4f orbital was treated based on the GGA+ U method (Dudarev et al., 1998). The value of U was set to be 5.4 eV in this study (Jiang et al., 2009, 2012). Structure optimization calculations were carried out until the residual forces were <0.02 eV/Å.

RESULTS AND DISCUSSION

Crystal Growth and Structure Determination

After washing the products inside the magnesia crucible with water to remove the solidified flux, we found that reddish-orange single crystals had grown on the inner wall of the tube (Figure 2) alongside with a plate-like pale-purple crystalline CeOCl byproduct. The EDS analysis of the reddish-orange crystals revealed the presence of Ce, Ca, Mg, and Ge in approximate atomic ratios of 1.9:1.0:2.1:2.6. The origin of the magnesium is the magnesia crucible that, apparently, was slightly dissolved by the flux during the reaction. Single-crystal X-ray diffraction analysis revealed that the product crystallized in the cubic system with $a = 12.5479(4)$ Å. The space group $Ia\bar{3}d$ (space group no. 230) was uniquely determined by the pattern of systematic absences in the intensity data and confirmed by structure solution. The product exhibits a garnet-type structure, wherein the asymmetric unit consists of one mixed Ce/Ca atomic site (Wyckoff site 24c), one Ge site (24d), one Mg site (16a), and one O site (96h). The composition of site 24c was determined by trial refinements of several models incorporating cationic elements determined by EDS to be present in the crystals (i.e., only Ce, Ca, Mg, and Ge). Modeling the site with mixed Ce/Ca occupancy resulted in the most reasonable model and is consistent with their similar ionic radii ($r_{\text{Ce}^{3+}} = 1.143$ Å, $r_{\text{Ca}^{2+}} = 0.97$ Å) (Shannon, 1976) and their observed bond distances to O [2.427(4) and 2.547(4) Å, respectively]. To maintain overall charge balance, the Ce and Ca occupancies were

TABLE 1 | Results of structural refinement of $\text{Ce}_2\text{CaMg}_2\text{Ge}_3\text{O}_{12}$ using single-crystal XRD data.

Crystal dimensions (mm^3)	$0.0807 \times 0.050 \times 0.030$
Crystal system	Cubic
Space group	$Ia\bar{3}d$ (#230)
a (\AA)	12.5487 (3)
V (\AA^3)	1976.04 (14)
Z	8
ρ_{cal} (g/cm^3)	5.235
Temperature (K)	301(2)
θ range ($^\circ$)	3.978–37.590
μ (mm^{-1})	18.765
Crystal dimensions (mm^3)	$0.080 \times 0.050 \times 0.030$
Collected reflections	17,162
Unique reflections	445
R_{int}	0.0645
GOF	1.286
R_1 for $F_o^2 > 2\sigma(F_o^2)$	0.0383
wR_2 for $F_o^2 > 2\sigma(F_o^2)$	0.0551
$\Delta\rho_{\text{max}}/\Delta\rho_{\text{min}}$ ($\text{e}/\text{\AA}^3$)	0.931/–1.069

TABLE 2 | Atomic coordinates and equivalent isotropic displacement parameters U_{eq} for $\text{Ce}_2\text{CaMg}_2\text{Ge}_3\text{O}_{12}$ obtained from the structure refinement using single-crystal XRD data.

Atom	Site	x	y	z	Occp.	U_{eq} ($\text{\AA}^2 \times 10^2$)
Ce ^a	24c	1/8	0	1/4	0.667	0.737 (15)
Ca ^a	24c	1/8	0	1/4	0.333	0.737
Mg	16a	0	0	0	1	0.75 (5)
Ge	24d	3/8	0	1/4	1	0.0660 (18)
O	96h	0.0948 (2)	0.1976 (3)	0.2852 (3)	1	0.68 (5)

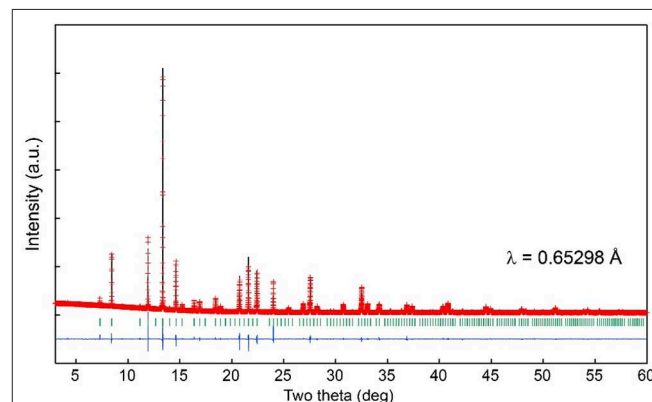
^aFor Ce and Ca atoms occupying the same site (24c), their site occupancies were fixed at 0.667 and 0.333, respectively, so that the sum of them was equal to unity. The U_{eq} values as well as the atomic coordinates were also constrained to the same values.

fixed at 2/3 Ce and 1/3 Ca. Trial refinements with Ce and Ca occupancies constrained to sum to 1.0 but otherwise free to vary, refined closely to these values, supporting the decision to fix the occupancies at 2/3 Ce and 1/3 Ca. All atoms were refined with anisotropic displacement parameters. The final refined chemical composition was $\text{Ce}_2\text{CaMg}_2\text{Ge}_3\text{O}_{12}$, which is consistent with the result of the EDS analysis. The final R_1 and wR_2 converged to reasonable values of 3.83 and 5.51%, respectively. The goodness-of-fit value was 1.29. The incorporation of Ce^{3+} ions into the structure was consistent with the reddish-orange sample color. Details of the structure refinement are listed in **Table 1**. Atomic coordinates and atomic displacement parameters are listed in **Table 2** and **Supplementary Table 1**, respectively. Selected bond distances and bond angles are compiled in **Table 3**.

Figure 3 shows the room-temperature synchrotron X-ray diffraction pattern collected from a powder sample obtained by finely grinding hand-picked single crystals. The model determined by the single-crystal structure analysis was used for the Rietveld refinement. The calculated pattern

TABLE 3 | Selected interatomic distances and bond angles of $\text{Ce}_2\text{CaMg}_2\text{Ge}_3\text{O}_{12}$ at 301 K.

Bond distance (\AA)		Bond angle (deg)	
Ce/Ca–O $\times 4$	2.427 (4)	Ce/Ca–O–Mg	97.48 (12)
Ce/Ca–O $\times 4$	2.547 (4)	Ce/Ca–O–Mg	101.26 (15)
Mg–O $\times 6$	2.102 (3)	Ce/Ca–O–Ge $\times 2$	95.60 (13)
Ge–O $\times 4$	1.766 (3)	Ce/Ca–O–Ce/Ca $\times 2$	101.13 (14)

**FIGURE 3** | Observed (crosses), calculated (upper solid line), and difference (lower solid line) plots obtained from the Rietveld analysis of the room temperature synchrotron X-ray powder diffraction data collected using ground single crystals of $\text{Ce}_2\text{CaMg}_2\text{Ge}_3\text{O}_{12}$. Vertical lines represent expected Bragg peak positions.

well-reproduced the observed pattern as the fitting converged smoothly with reasonable reliability indexes, $R_{\text{wp}} = 5.37$, $R_{\text{B}} = 3.45$, and $R_{\text{F}} = 2.92$. The final refined crystallographic data, including the atomic coordinates and isotropic displacement parameters are listed in **Supplementary Table 2**. The results are consistent with the results obtained from the single-crystal structure analysis.

Solid State Reaction

Synthesis of a polycrystalline sample of $\text{Ce}_2\text{CaMg}_2\text{Ge}_3\text{O}_{12}$ was attempted by solid-state reactions using a stoichiometric mixture of CeO_2 , CaCO_3 (or CaO), MgO , and GeO_2 . The reactions were carried out under vacuum, with mixed H_2 (20%)- Ar (80%) gas or N_2 gas atmospheres at temperatures between 900 and $1,300^\circ\text{C}$. Unfortunately, none of the reaction conditions we examined yielded the target phase; but a substantial amount of unreacted CeO_2 always remained in the products (see **Supplementary Figure 1**). A garnet structure was obtained as a minor phase at $1,300^\circ\text{C}$ in the N_2 gas atmosphere; however, the lattice parameter of the garnet phase was smaller by 0.5% compared with that for $\text{Ce}_2\text{CaMg}_2\text{Ge}_3\text{O}_{12}$ and the product was dark grayish-green. Therefore, if Ce atoms were incorporated into the lattice, the garnet phase obtained by solid state reaction should have a lower Ce concentration than that of $\text{Ce}_2\text{CaMg}_2\text{Ge}_3\text{O}_{12}$. Further heating at the same temperature after regrinding and pelletizing resulted in a partial decomposition of the garnet phase and an increase in the amount of CeO_2 ,

suggesting that the garnet phase was metastable under these reaction conditions.

Stability of the Garnet Structure

As described earlier, the garnet structure can accommodate a wide range of elements in the three different cation sites, but the underlying stability of the garnet structure, including its tolerance for RE ions, is not yet well-understood. Our present germanate garnet exhibited an unusual occupancy of two-thirds of the A sites by Ce^{3+} ions, a Ce^{3+} concentration substantially higher than the 56 at.% Ce^{3+} -doping concentration found in $Y_{1-x}Ce_xFe_5O_{12}$ ($x = 1.7$) (Rongjin et al., 2013). Very recently, Song et al. have formulated the tolerance factor (τ) of the garnet structure (Song et al., 2019), which is analogous to the Goldschmidt tolerance factor describing the relationship of the chemical compositions and structural stability in perovskites (Goldschmidt, 1926). The τ of the garnet structure is expressed as

$$\tau = \frac{3\sqrt{(r_B + r_O)^2 + \frac{4}{9}(r_A + r_O)^2}}{2(r_C + r_O)} \quad (1)$$

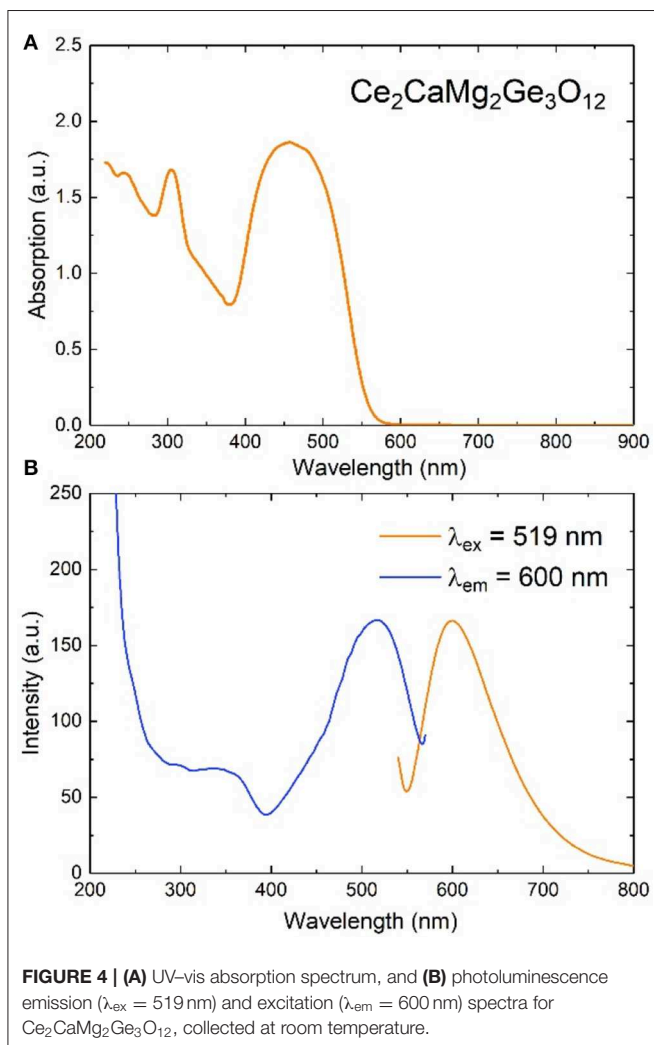


FIGURE 4 | (A) UV-vis absorption spectrum, and **(B)** photoluminescence emission ($\lambda_{ex} = 519$ nm) and excitation ($\lambda_{em} = 600$ nm) spectra for $Ce_2CaMg_2Ge_3O_{12}$, collected at room temperature.

where r_A , r_B , r_C , and r_O represent the ionic radii of the A , B , C site cations and O^{2-} ion, respectively. The tolerance factor calculated for more than 100 garnet compounds falls within the range of 0.75–1.33. For the formula $RE_3B_2C_3O_{12}$ ($RE = La-Lu$, Y ; $B = C = Fe, Al, Ga$), the τ values systematically increase toward unity with decreasing size of the RE ions, e.g., 0.76–0.93 from La to Lu for $RE_3Al_5O_{12}$ and 0.89–1.02 for $RE_3Fe_5O_{12}$ (Song et al., 2019). This is consistent with the general trend observed for their structural stability when containing RE ions. The formula $RE_2CaMg_2Ge_3O_{12}$ ($RE = La-Lu, Y$), including hypothetical compositions, exhibits a similar size dependence of the tolerance

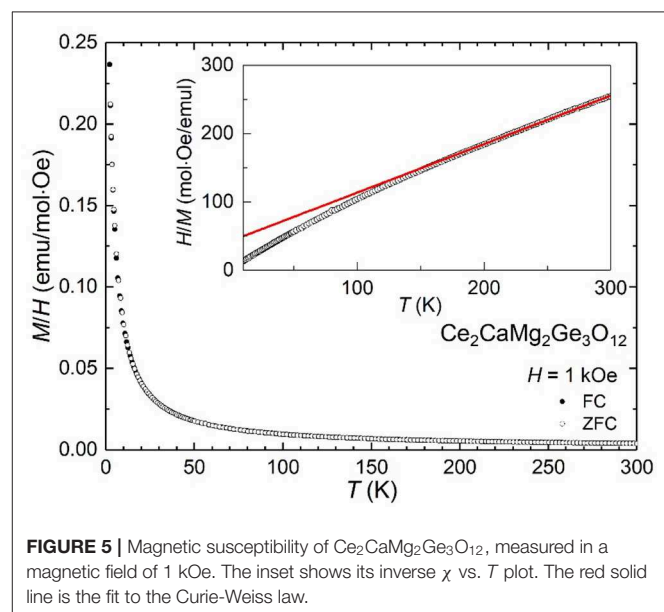


FIGURE 5 | Magnetic susceptibility of $Ce_2CaMg_2Ge_3O_{12}$, measured in a magnetic field of 1 kOe. The inset shows its inverse χ vs. T plot. The red solid line is the fit to the Curie-Weiss law.

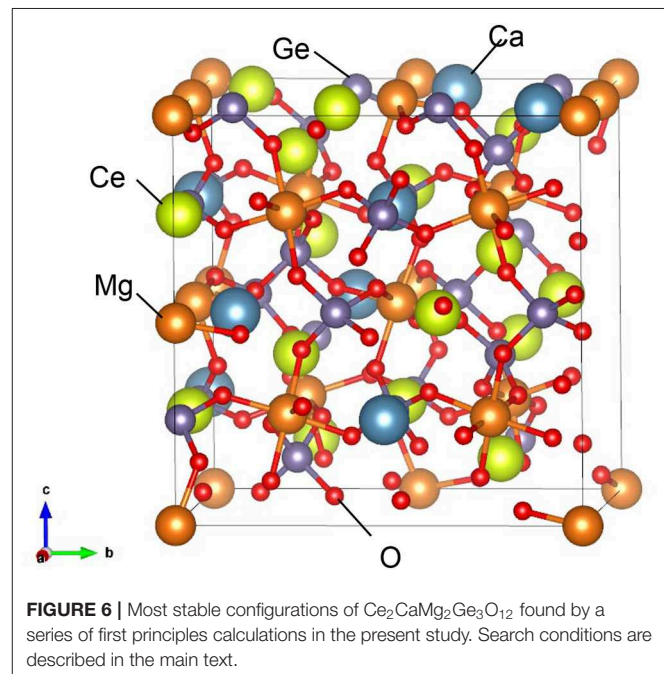


FIGURE 6 | Most stable configurations of $Ce_2CaMg_2Ge_3O_{12}$ found by a series of first principles calculations in the present study. Search conditions are described in the main text.

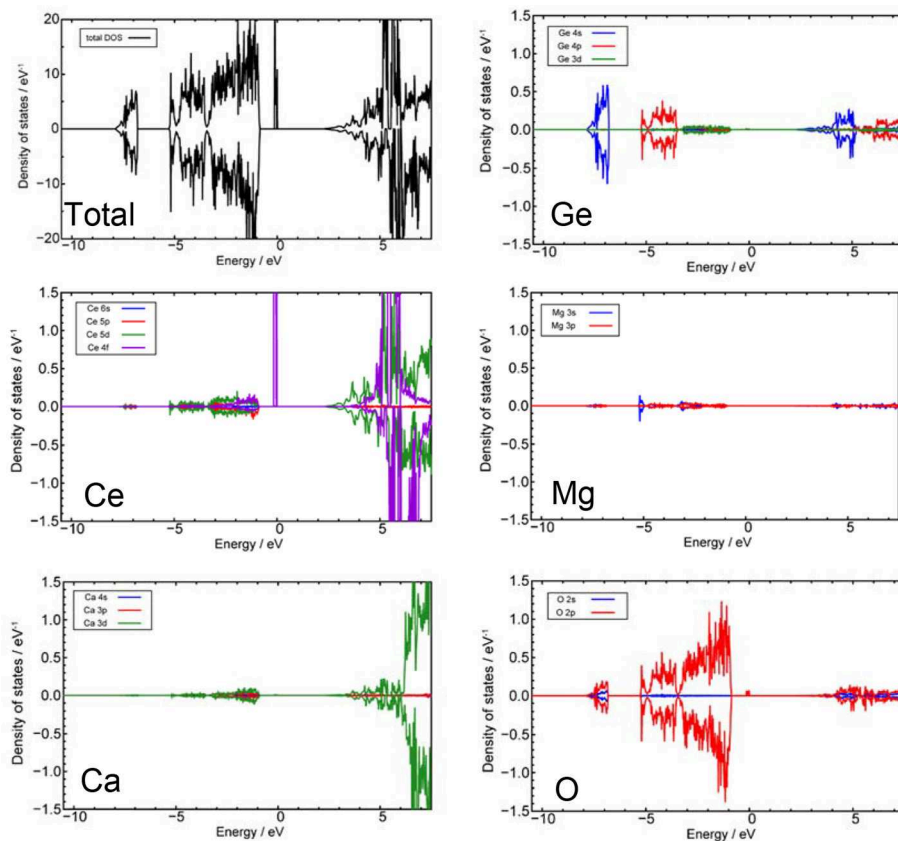


FIGURE 7 | Total and projected partial density of states calculated from the model shown in **Figure 6**. The energy level of a valence band top is set to be 0 eV on the horizontal axes. Positive and negative values of the vertical axes indicate the DOS of up-spin and down-spin, respectively. Blue, red, green, and purple lines indicate the *s*, *p*, *d*, and *f* orbitals of each element, respectively.

factor, but the τ values range from 1.06 for La, through 1.07 for Ce, to 1.15 for Lu. The stabilization of $\text{Ce}_2\text{CaMg}_2\text{Ge}_3\text{O}_{12}$ with a τ value close to unity seems to be compatible with the geometric requirements for the garnet structure. However, a favorable tolerance factor does not assure the success of the target phase formation via chemical synthesis. In fact, the solid-state reactions we examined to obtain $\text{Ce}_2\text{CaMg}_2\text{Ge}_3\text{O}_{12}$ were not successful. At present, the reason for the large amount of Ce ions incorporated into the garnet lattice is unclear; however, it is likely that the molten salts used in this study play a crucial role in stabilizing the phase under the flux reaction conditions. From the PXRD data of the products obtained by solid state reactions, it is apparent that CeO_2 was not fully consumed in the reactions, indicating its low reactivity and slow atomic diffusion even at high temperatures. In the flux reaction, the $\text{BaCl}_2\text{--CaCl}_2$ salt likely dissolves CeO_2 powder at a relatively low temperature, where the fact that the starting materials are now in solution is expected to decrease considerably the activation energy for reaction between the starting materials and thus yield the target garnet phase. We surmise that the Ca-Cl melt at high temperatures under vacuum acts as a reducing agent for Ce ions, likely forming Cl_2 . The formation of Ce^{3+} in the halide melt favors the stabilization of $\text{Ce}_2\text{CaMg}_2\text{Ge}_3\text{O}_{12}$ as well as of the byproduct CeOCl . Sulfur,

which was a starting material for the flux reaction, was not found to significantly contribute to either the reduction of Ce ions nor to the formation of $\text{Ce}_2\text{CaMg}_2\text{Ge}_3\text{O}_{12}$. Performing the flux crystal growth in the absence of sulfur results in the same mixed product formation.

Optical and Magnetic Properties

Figure 4A shows the UV–vis absorption spectrum collected for $\text{Ce}_2\text{CaMg}_2\text{Ge}_3\text{O}_{12}$, exhibiting a clear absorption edge at around 560 nm. An extrapolation of the linear portion of the absorption curve to the *x*-axis indicates an optical band gap of $E_g = 2.22$ eV. This steep increase in the absorption is followed by two broad sub-bands centered at 458 and 305 nm, also observed in the UV–vis absorption curves of YAG:Ce. These two absorption peaks can be assigned to the optical transitions from the Ce *4f* ground state to the lowest and second-lowest excited states of the Ce *5d* orbitals (*5d*₁ and *5d*₂, respectively) (Bachmann et al., 2009). A third weak peak at around 250 nm is probably due to defects or impurities. The lowest absorption is in the blue spectral region, which results in the reddish orange color of the garnet compound. The photoluminescence emission (PE) and excitation (PLE) spectra of $\text{Ce}_2\text{CaMg}_2\text{Ge}_3\text{O}_{12}$ are shown in **Figure 4B**. The PE spectrum excited at 519 nm contains a broad

band centered around 600 nm, which could be assigned to the transition from the $5d_1$ level to the two $4f$ levels split by spin-orbit coupling into ${}^2F_{5/2}$ and ${}^2F_{7/2}$. The maximum value of the emission band for $\text{Ce}_2\text{CaMg}_2\text{Ge}_3\text{O}_{12}$ is red-shifted compared to that of $\text{Y}_2\text{Mg}_3\text{Ge}_3\text{O}_{12}:\text{Ce}(2\%)$ (Jiang et al., 2010) but comparable to that for $\text{Gd}_2\text{Mg}_3\text{Ge}_3\text{O}_{12}:\text{Ce}(2\%)$ (Wu et al., 2007).

Figure 5 shows the temperature evolution of the magnetic susceptibility χ ($= M/H$) measured in a magnetic field $H = 1$ kOe. Both the ZFC and FC data increase smoothly with decreasing temperature, indicative of a paramagnetic state persisting down to low temperatures. No significant difference between the ZFC and FC data was observed in the temperature range between 10 and 300 K. Fitting $\chi(T)$ to the Curie–Weiss law yields $C = 1.407(4)$ (emu K/mol) and $\theta = -59.9(9)$ K, where C and θ stand for the Curie and Weiss constants, respectively. The C value is somewhat smaller than the theoretical value expected from two mol Ce^{3+} ions with ${}^2F_{5/2}$ per formula unit. The negative θ value suggests that Ce^{3+} ions are antiferromagnetically coupled to each other. The absence of a long-range magnetic order is probably due to a random distribution of Ce and Ca atoms on the $24c$ site.

Theoretical Calculations

From the experimental crystal structure analysis of $\text{Ce}_2\text{CaMg}_2\text{Ge}_3\text{O}_{12}$, Ce, and Ca ions are found to occupy the A site of the $A_3B_2C_3O_{12}$ garnet structure. In first principles calculations using structure models under periodic boundary conditions, mixed occupancy of atomic sites cannot be directly computed. Therefore, we initially determined the preferred distribution of Ce and Ca ions on the A site with a ratio of 2:1 in a fixed size model having the garnet structure. We chose a primitive unit cell of the garnet structure as a base model. Structure models having symmetrically non-equivalent configurations of Ce and Ca ions were constructed. In total, 20 independent configurations of Ce and Ca ions on the A -site were found from the base model using the CLUPAN code (Seko et al., 2009). The mesh size of k -point sampling was $3 \times 3 \times 3$ in the Brillouin zone of the input structure models. We compared the total energies of these models obtained by structure optimization calculations.

From the series of total energy calculations of $\text{Ce}_2\text{CaMg}_2\text{Ge}_3\text{O}_{12}$ models, the most stable configuration that was found is shown in **Figure 6**. We analyzed the electronic structures of this model. **Figure 7** shows total density of states (tDOS) and projected partial density of states (pDOS) of each constituent element. In **Figure 7**, the energy level of a valence band top is set to be 0 eV on the horizontal axes. Positive and negative values on the vertical axes indicate the DOS of up-spin and down-spin, respectively. The tDOS values show that the calculated band gap is about 2.2 eV, which is in a good agreement with the value estimated from the UV–vis absorption spectrum. It can be clearly seen that very sharp spikes of the DOS exist at the topmost energy levels of the occupied states. Such sharp DOS peaks indicate strong localization states of the electron orbitals. From the pDOS values, we can see that these peaks originate from the occupied $4f$ orbital of the Ce^{3+} ions. The DOS near the conduction band bottom seems to be mainly composed

of an unoccupied $5d$ orbital of Ce^{3+} ions and a $4s$ orbital of the Ge^{4+} ions.

CONCLUSION

We have successfully synthesized a new metastable germanate garnet, $\text{Ce}_2\text{CaMg}_2\text{Ge}_3\text{O}_{12}$, using a flux crystal growth method. Reddish-orange single crystals were grown in a reactive MgO crucible; however, the polycrystalline sample could not be prepared via a solid state reaction. Flux reactions are clearly useful for extending the garnet family to compositions that include the early lanthanide metals, especially those larger than Gd, which have been less explored. The PL intensity was so weak that it could not be confirmed visually; this is probably due to Ce^{3+} -concentration quenching effects or photoionization involving a charge transfer between Ce^{3+} and Ge^{4+} (Blasse et al., 1991; Pinelli et al., 2004). Work to synthesize La or RE ($<\text{Ce}^{3+}$)-doped $\text{Ce}_2\text{CaMg}_2\text{Ge}_3\text{O}_{12}$ and the substitution of Si for Ge, which would enhance PL properties, is ongoing.

DATA AVAILABILITY STATEMENT

The datasets generated for this study can be found in the Cambridge Crystallographic Data Centre (<https://www.ccdc.cam.ac.uk/structures/>) under the identifier 1969400.

AUTHOR CONTRIBUTIONS

The manuscript was written through contributions of all authors. All authors have given approval to the final version of the manuscript.

FUNDING

Research grants from JSPS KAKENHI (Grant Nos. 15H02024, 16H06438, 16H06441, 19H02594, 19H04711, 17H05493, 16H06439, and 16K21724) and Innovative Science and Technology Initiative for Security, ATLA, Japan. Research Grant from UofSC (NSF grant DMR-1806279).

ACKNOWLEDGMENTS

We thank Dr. Y. Katsuya, Dr. M. Tanaka, and Prof. O. Sakata for their assistance in performing the SXRDX experiments at SPring-8 (Proposal No. 2018B4502, 2019A4501).

SUPPLEMENTARY MATERIAL

The Supplementary Material for this article can be found online at: <https://www.frontiersin.org/articles/10.3389/fchem.2020.00091/full#supplementary-material>

CIF files of $\text{Ce}_2\text{CaMg}_2\text{Ge}_3\text{O}_{10}$ based on single crystal XRD data. Anisotropic displacement parameters for $\text{Ce}_2\text{CaMg}_2\text{Ge}_3\text{O}_{10}$. Crystallographic data obtained from the Rietveld refinement against the SXRDX data. Powder XRD data collected from the products of the solid state reactions.

REFERENCES

- Awaka, J., Kijima, N., Hayakawa, H., and Akimoto, J. (2009). Synthesis and structure analysis of tetragonal $\text{Li}_7\text{La}_3\text{Zr}_2\text{O}_{12}$ with the garnet-related type structure. *J. Solid State Chem.* 182, 2046–2052. doi: 10.1016/j.jssc.2009.05.020
- Bachmann, V. M., Ronda, C., and Meijerink, A. (2009). Temperature quenching of yellow Ce^{3+} luminescence in YAG:Ce. *Chem. Mater.* 21, 2077–2084. doi: 10.1021/cm8030768
- Blasse, G., Schipper, W., and Hamelink, J. J. (1991). On the quenching of the luminescence of the trivalent cerium ion. *Inorganica Chimica Acta.* 189, 77–80.
- Blöchl, P. E. (1994). Projector augmented-wave method. *Phys. Rev. B Condens. Matter.* 50, 17953–17979. doi: 10.1103/PhysRevB.50.17953
- Bruker AXS Inc. (2016). *APEX3 Version 2016.5-0 and SAINT+ Version 8.37A*. Madison, WI: Bruker AXS Inc.
- Bugaris, D. E., and zur Loye, H. C. (2012). Materials discovery by flux crystal growth: quaternary and higher order oxides. *Angew. Chem. Int. Ed. Engl.* 51, 3780–3811. doi: 10.1002/anie.201102676
- Dudarev, S. L., Botton, G. A., Savrasov, S. Y., Humphreys, C., and Sutton, A. P. (1998). Electron-energy-loss spectra and the structural stability of nickel oxide: an LSDA+U study. *Phys. Rev. B* 57, 1505–1509. doi: 10.1103/PhysRevB.57.1505
- Dukhovskaya, E. L., Saksonov, Y. G., and Titova, A. G. (1973). Oxygen parameters of certain compounds of the garnet structure. *Izvestiya Akademii Nauk SSSR Neorganicheskii Mater.* 9, 809–813.
- Garskaite, E., Sakirzanovas, S., Kareiva, A., Glaser, J., and Meyer, H.-J. (2007). Synthesis and structure of europium aluminium garnet (EAG). *Zeitschrift für anorganische und allgemeine Chemie.* 633, 990–993. doi: 10.1002/zaac.200700027
- Geller, S. (1967). Crystal chemistry of the garnets. *Zeitschrift für Kristallographie - Crystalline Mater.* 125, 1–47. doi: 10.1524/zkri.1967.125.125.1
- Goldschmidt, V. M. (1926). Die gesetze der kristallochemie. *Die Naturwissenschaften.* 14, 477–485.
- Guo, L., Huang, K., Chen, Y., Li, G., Yuan, L., Peng, W., et al. (2011). Mild hydrothermal synthesis and ferrimagnetism of $\text{Pr}_3\text{Fe}_5\text{O}_{12}$ and $\text{Nd}_3\text{Fe}_5\text{O}_{12}$ garnets. *J. Solid State Chem.* 184, 1048–1053. doi: 10.1016/j.jssc.2011.03.010
- Hübschle, C. B., Sheldrick, G. M., and Dittrich, B. (2011). ShelXle: a Qt graphical user interface for SHELXL. *J. Appl. Crystallogr.* 44, 1281–1284. doi: 10.1107/S0021889811043202
- Izumi, F., and Momma, K. (2007). Three-dimensional visualization in powder diffraction. *Solid State Phenomena.* 130, 15–20. doi: 10.4028/www.scientific.net/SSP.130.15
- Jiang, H., Gomez-Abal, R. I., Rinke, P., and Scheffler, M. (2009). Localized and itinerant states in lanthanide oxides united by GW @ LDA+U. *Phys. Rev. Lett.* 102:126403. doi: 10.1103/PhysRevLett.102.126403
- Jiang, H., Rinke, P., and Scheffler, M. (2012). Electronic properties of lanthanide oxides from the GW perspective. *Phys. Rev. B* 86:125115. doi: 10.1103/PhysRevB.86.125115
- Jiang, Z., Wang, Y., and Wang, L. (2010). Enhanced yellow-to-orange emission of Si-Doped $\text{Mg}_3\text{Y}_2\text{Ge}_3\text{O}_{12}:\text{Ce}^{3+}$ garnet phosphors for warm white light-emitting diodes. *J. Electrochem. Soc.* 157:J155. doi: 10.1149/1.3328530
- Kasper, H. M. (1969). Series of rare earth garnets $\text{Ln}_3+3\text{M}_2\text{Li}+3\text{O}_{12}$ (M=Te, W). *Inorgan. Chem.* 8, 1000–1002. doi: 10.1021/ic50074a058
- Komori, T., Sakakura, T., Takenaka, Y., Tanaka, K., and Okuda, T. (2009a). Tripraseodymium penta-iron(III) dodeca-oxide, $\text{Pr}_3\text{Fe}_5\text{O}_{12}$: a synchrotron radiation study. *Acta Crystallogr. Sect. E Struct. Rep. Online* 65:i73. doi: 10.1107/S1600536809038100
- Komori, T., Sakakura, T., Takenaka, Y., Tanaka, K., and Okuda, T. (2009b). Trineodymium(III) penta-iron(III) dodeca-oxide, $\text{Nd}_3\text{Fe}_5\text{O}_{12}$. *Acta Crystallogr. Sect. E Struct. Rep. Online* 65:i72. doi: 10.1107/S1600536809036794
- Krause, L., Herbst-Irmer, R., Sheldrick, G. M., and Stalke, D. (2015). Comparison of silver and molybdenum microfocus X-ray sources for single-crystal structure determination. *J. Appl. Crystallogr.* 48, 3–10. doi: 10.1107/S1600576714022985
- Kresse, G., and Furthmüller, J. (1996a). Efficient iterative schemes for ab initio total-energy calculations using a plane-wave basis set. *Phys. Rev. B Condens. Matter.* 54, 11169–11186. doi: 10.1103/PhysRevB.54.11169
- Kresse, G., and Furthmüller, J. (1996b). Efficiency of ab-initio total energy calculations for metals and semiconductors using a plane-wave basis set. *Comput. Mater. Sci.* 6, 15–50. doi: 10.1016/0927-0256(96)00008-0
- Kresse, G., and Hafner, J. (1993). Ab initio molecular dynamics for liquid metals. *Phys. Rev. B Condens. Matter.* 47, 558–561. doi: 10.1103/PhysRevB.47.558
- Kresse, G., and Joubert, D. (1999). From ultrasoft pseudopotentials to the projector augmented-wave method. *Phys. Rev. B.* 59, 1758–1775. doi: 10.1103/PhysRevB.59.1758
- Lévy, D., and Barbier, J. (1999). Normal and inverse garnets: $\text{Ca}_3\text{Fe}_2\text{Ge}_3\text{O}_{12}$, $\text{Ca}_3\text{Y}_2\text{Ge}_3\text{O}_{12}$ and $\text{Mg}_3\text{Y}_2\text{Ge}_3\text{O}_{12}$. *Acta Crystallogr. Sect. C Cryst. Struct. Commun.* 55, 1611–1614. doi: 10.1107/S0108270199007854
- Malysa, B., Meijerink, A., and Jüstel, T. (2018). Temperature dependent Cr^{3+} photoluminescence in garnets of the type $\text{X}_3\text{Sc}_2\text{Ga}_3\text{O}_{12}$ (X = Lu, Y, Gd, La). *J. Luminescence* 202:523–531. doi: 10.1016/j.jlumin.2018.05.076
- Muñoz-García, A. B., Pascual, J. L., Barandiarán, Z., and Seijo, L. (2010). Structural effects and 4f–5d transition shifts induced by La codoping in Ce-doped yttrium aluminum garnet: first-principles study. *Phys. Rev. B.* 82:064114. doi: 10.1103/PhysRevB.82.064114
- Muñoz-García, A. B., and Seijo, L. (2010). Structural, electronic, and spectroscopic effects of Ga codoping on Ce-doped yttrium aluminum garnet: first-principles study. *Phys. Rev. B.* 82:184118. doi: 10.1103/PhysRevB.82.184118
- Murugan, R., Weppner, W., Schmid-Beurmann, P., and Thangadurai, V. (2008). Structure and lithium ion conductivity of garnet-like $\text{Li}_5\text{La}_3\text{Sb}_2\text{O}_{12}$ and $\text{Li}_6\text{SrLa}_2\text{Sb}_2\text{O}_{12}$. *Mater. Res. Bulletin* 43, 2579–2591. doi: 10.1016/j.materresbull.2007.10.035
- Perdew, J. P., Ruzsinszky, A., Csonka, G. I., Vydrov, O. A., Scuseria, G. E., Constantin, L. A., et al. (2008). Restoring the density-gradient expansion for exchange in solids and surfaces. *Phys. Rev. Lett.* 100:136406. doi: 10.1103/PhysRevLett.100.136406
- Pinelli, S., Bigotta, S., Toncelli, A., Tonelli, M., Cavalli, E., and Bovero, E. (2004). Study of the visible spectra of $\text{Ca}_3\text{Sc}_2\text{Ge}_3\text{O}_{12}$ garnet crystals doped with Ce^{3+} or Pr^{3+} . *Optic. Mater.* 25, 91–99. doi: 10.1016/S0925-3467(03)0231-3
- Reinen, D. (1964). Die Lichtabsorption des Co^{2+} und Ni^{2+} in oxidischen Festkörpern mit Granatstruktur. *I. Zeitschrift für anorganische und allgemeine Chemie* 327, 238–252. doi: 10.1002/zaac.19643270317
- Rongjin, J., Wenhui, Y., Caixiang, F., and Yanwei, Z. (2013). Glycothermal synthesis of heavily Ce-doped YIG nanocrystals and their microstructures and magnetic properties. *J. Mater. Chem. C* 1:1763. doi: 10.1039/c2tc00335j
- Sawada, H. (1997). Electron density study of garnets: $\text{Z}_3\text{Ga}_5\text{O}_{12}$; Z=Nd, Sm, Gd, Tb. *J. Solid State Chem.* 132, 300–307. doi: 10.1006/jssc.1997.7462
- Sawada, K., Nakamura, T., and Adachi, S. (2016). Europium gallium garnet ($\text{Eu}_3\text{Ga}_5\text{O}_{12}$) and Eu_3GaO_6 : synthesis and material properties. *J. Appl. Phys.* 120:143102. doi: 10.1063/1.4964444
- Seko, A., Koyama, Y., and Tanaka, I. (2009). Cluster expansion method for multicomponent systems based on optimal selection of structures for density-functional theory calculations. *Phys. Rev. B* 80:165122. doi: 10.1103/PhysRevB.80.165122
- Setlur, A. A., Heward, W. J., Gao, Y., Srivastava, A. M., Chandran, R. G., Shankar, M. V., et al. (2006). Crystal chemistry and luminescence of Ce^{3+} -doped $\text{Lu}_2\text{CaMg}_2(\text{Si},\text{Ge})_3\text{O}_{12}$ and its use in LED based lighting. *Chem. Mater.* 18, 3314–3322. doi: 10.1021/cm060898c
- Shannon, R. D. (1976). Revised effective ionic radii and systematic studies of interatomic distances in halides and chalcogenides. *Acta Crystallogr. Sect. A.* 32, 751–767. doi: 10.1107/S0567739476001551
- Shao, Q., Dong, Y., Jiang, J., Liang, C., and He, J. (2011). Temperature-dependent photoluminescence properties of (Y, Lu) $_3\text{Al}_5\text{O}_{12}:\text{Ce}^{3+}$ phosphors for white LEDs applications. *J. Luminescence* 131, 1013–1015. doi: 10.1016/j.jlumin.2011.01.013
- Sheldrick, G. M. (2015). SHELXT - integrated space-group and crystal-structure determination. *Acta Crystallogr. A Found Adv.* 71, 3–8. doi: 10.1107/S2053273314026370
- Song, Z., Zhou, D., and Liu, Q. (2019). Tolerance factor and phase stability of the garnet structure. *Acta Crystallogr. C Struct. Chem.* 75, 1353–1358. doi: 10.1107/S2053229619011975

- Tauber, A., Banks, E., and Kedesdy, H. (1958). Synthesis of germanate garnets. *Acta Crystallogr.* 11, 893–894. doi: 10.1107/S0365110X58002528
- Ueda, J., Dorenbos, P., Bos, A. J. J., Meijerink, A., and Tanabe, S. (2015). Insight into the thermal quenching mechanism for $Y_3Al_5O_{12}:Ce^{3+}$ through thermoluminescence excitation spectroscopy. *J.Phys. Chem. C* 119, 25003–25008. doi: 10.1021/acs.jpcc.5b08828
- Wu, J. L., Gundiah, G., and Cheetham, A. K. (2007). Structure–property correlations in Ce-doped garnet phosphors for use in solid state lighting. *Chem. Phys. Lett.* 441, 250–254.
- Zhiguo, X., and Meijerink, A. (2017). Ce^{3+} -doped garnet phosphors: composition modification, luminescence properties and applications. *Chem. Soc. Rev.* 46, 275–299. doi: 10.1039/C6CS00551A

Conflict of Interest: The authors declare that the research was conducted in the absence of any commercial or financial relationships that could be construed as a potential conflict of interest.

Copyright © 2020 Chen, Yan, Kuwabara, Smith, Iwasa, Ogino, Matsushita, Tsujimoto, Yamaura and zur Loye. This is an open-access article distributed under the terms of the Creative Commons Attribution License (CC BY). The use, distribution or reproduction in other forums is permitted, provided the original author(s) and the copyright owner(s) are credited and that the original publication in this journal is cited, in accordance with accepted academic practice. No use, distribution or reproduction is permitted which does not comply with these terms.